Position of Synaptotagmin I at the Membrane Interface: Cooperative Interactions of Tandem C2 Domains†

Dawn Z. Herrick,‡ Stephenie Sterbling,‡ Katie A. Rasch,§ Anne Hinderliter,§ and David S. Cafiso*,‡

Department of Chemistry and Biophysics Program, University of Virginia, Charlottesville, Virginia, and Department of Pharmaceutical Sciences, North Dakota State University, Fargo, North Dakota

Received May 3, 2006; Revised Manuscript Received June 20, 2006

ABSTRACT: Synaptotagmin I is a synaptic vesicle associated membrane protein that appears to regulate Ca^{2+}-mediated exocytosis. Here, the Ca^{2+}-dependent membrane interactions of a water soluble fragment of synaptotagmin I (C2AB) that contains its two C2 domains (C2A and C2B) were determined using site-directed spin labeling. Membrane depth parameters were obtained for 19 spin-labeled mutants of C2AB when bound to phosphatidylcholine and phosphatidylserine membranes, and these distance constraints were used in combination with the high-resolution structures of C2A and C2B to generate a model for the membrane orientation and position of synaptotagmin at the bilayer interface. Both C2A and C2B bind to the membrane interface with their first and third Ca^{2+} binding loops penetrating the membrane interface. The polybasic face of C2B does not interact with the membrane lipid but is available for electrostatic interaction with other components of the fusion machinery. When compared to positions determined previously for the isolated domains, both C2A and C2B have similar orientations; however, the two domains are positioned deeper into the bilayer interior when present in the tandem construct. These data indicate that C2A and C2B do not act independently but influence their mutual membrane penetration. This may explain the occurrence of multiple C2 domains in proteins that function in membrane trafficking and repair.

Regulated exocytosis is a vital cellular process that is coordinated by a large number of protein components. The SNAREs are central to the fusion process and form a four helix bundle that tethers the synaptic and plasma membranes together (*1*−*3*). In neuronal membrane fusion, Ca^{2+}-dependent fusion is not regulated directly by the SNAREs but appears to be regulated by syntaptotagmin I (sytI[1]), a synaptic vesicle membrane protein that has two C2 domains (*4*). Synaptotagmin I is associated with the synaptic vesicle through a single transmembrane segment near its *N*-terminus as well as through protein acylation (*5*) (Figure 1). Its two C2 domains are located toward the *C*-terminal side of the protein, and each domain when expressed and isolated separately will bind independently to membranes containing a negatively charged lipid in a Ca^{2+}-dependent fashion. Synaptotagmin I has also been reported to bind to SNAREs through its C2 domains, although reports vary regarding the Ca^{2+}-dependence of this interaction (*6*, *7*).

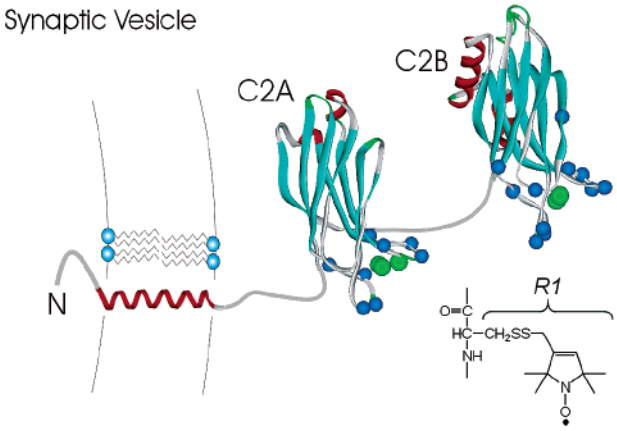

FIGURE 1: Synaptotagmin I and its two tandem C2 domains. This protein is anchored to the synaptic vesicle membrane by a single transmembrane helical segment near its *N*-terminus. The C2A domain includes residues 156−244, whereas residues 286−418 encompass the C2B domain. In this study, 19 single cysteine mutants of a water soluble fragment of synaptotagmin I (136−418) (96−421 expressed) were produced (Cα positions shown in blue), expressed, and derivatized with a methanethiosulfonate spin label to attach the side chain R1.

There are a number of proteins that have multiple C2 domains that have been implicated in membrane trafficking and repair. The copines are a family of ubiquitous proteins containing two C2 domains involved in Ca^{2+}-dependent membrane binding (*8*). Tricalbins are a recently discovered family of proteins derived from yeast, which appear to have

† This work was supported by National Institutes of Health Grants GM 62035 (to D.S.C.), GM72694 (to D.S.C.), and GM64443 (to A.H.) and the ACS Petroleum Research Fund type G (to A.H.).

* To whom correspondence should be addressed. Tel: 434-924-3067. Fax: 434-924-3567. E-mail: cafiso@virginia.edu.

‡ University of Virginia.

§ North Dakota State University.

[1] Abbreviations: EPR, electron paramagnetic resonance spectroscopy; LUV, large unilamellar vesicle; $PI(4,5)P_2$, phosphatidylinositol 4-5 bisphosphate; POPC, palmitoyloleoylphosphatidylcholine; POPS, palmitoyloleoylphosphatidylserine; R1, spin-labeled side chain produced by the derivatization of a cysteine with a methanethiosulfonate spin label; SDSL, site-directed spin labeling; sytI, synaptotagmin I; sytIC2AB or C2AB, soluble fragment of syaptotagmin I containing C2A and C2B; synIC2A or C2A, synaptotagmin I C2A domain; sytIC2B or C2B, synaptotagmin I C2B domain.

10.1021/bi060874j CCC: $33.50
Published on Web 07/25/2006

an *N*-terminal transmembrane segment and three C2 domains (*9*). These proteins are thought to be homologues of synaptotagmin that are involved in membrane trafficking. As many as six C2 domains are seen in the ferlins, a family of proteins that play a role in membrane repair (*10*−*12*).

At the present time, the role of multiple C2 domains is not known. In sytI, multiple domains may function to enhance membrane binding, or they might display different lipid specificities. There is evidence for both functions. For example, the first C2 domain, C2A, is reported to show preferential binding in a Ca^{2+}-dependent manner to phosphatidylserine (PS)-containing membranes. The second, more *C*-terminal C2 domain, C2B, also binds PS-containing membranes but shows strong affinity toward membranes containing phosphatidylinositol 4-5 bisphosphate (PI(4,5)-P_2) (*13*). There are a number of reports indicating that the two domains act synergistically. Neither C2A nor C2B displays strong Ca^{2+}-dependent binding to isolated chromaffin granules when expressed as isolated domains, but they bind strongly to these membranes when expressed together in an intact water-soluble fragment of sytI (*14*). There is also evidence that the domains, particularly C2B, bind differently in the presence of the other domain and that mutations within a construct containing the two domains are not additive (*6*, *15*, *16*).

In the present work, we examine the position of a fragment of sytI that contains both C2A and C2B (sytIC2AB) at the interface of membranes containing the acidic lipid phosphatidylserine (PS). We use an approach termed site-directed spin labeling (SDSL) that involves the use of EPR spectroscopy to study mutants of sytIC2AB that contain the nitroxide side chain, R1 (Figure 1). In previous work, we used this approach to determine the membrane position and orientation of C2A and C2B from sytI when expressed as individual domains (*17*, *18*). In the present study, we express, purify, and make measurements on 19 mutants of sytIC2AB. The distance constrains that are obtained are used to generate a model for the domains at the interface. We find that the orientations of C2A and C2B in sytIC2AB are similar to that found in the two isolated domains, with both the first and third Ca^{2+} binding loops penetrating the membrane interface. However, both C2A and C2B appear to penetrate more deeply into the membrane when they are present together than when they are isolated domains. This work indicates that the two domains act synergistically to promote their mutual membrane insertion. Both the membrane orientation of these domains and their penetration suggest a molecular role for sytI in membrane fusion.

MATERIALS AND METHODS

DNA Modification. The DNA of rat sytIC2AB (P21707), in the vector pGEX-KG (*14*), encoding amino acid residues 96−421 was obtained from Dr. Carl Creutz (Pharmacology Department, University of Virginia). All DNA modifications followed published protocols (*19*). The single native cysteine residue at position 277 was mutated to alanine by typical polymerase chain reaction (PCR) strategies. Either a two-step PCR process or a QuickChange Site-Directed Mutagenesis Kit (Stratagene) was used to produce single-cysteine mutants of C2AB. Individual cysteine residues were introduced at the following positions in the C2A domain of C2AB: 171, 173, 174, 202, 231, 234, 236, and 239 and in the C2B domain of C2AB: 297, 300, 304, 305, 306, 327, 334, 367, 368, 369, and 370. All cysteine substitutions were confirmed by DNA sequencing.

Protein Expression and Purification. The synaptotagmin I C2AB construct was encoded in frame with glutathione *S*-transferase (GST). The mutant plasmids for GST-C2AB were transformed into BL21(DE3)pLys*S* cells (Promega), and cell growth and protein purification were carried out as described previously (*18*). The GST-C2AB fusion protein was purified by affinity chromatography as described for C2B (*18*). Two additional GSTrap FF columns (Amersham Biosciences) were added in series prior to elution to scavenge the residual GST protein. In addition, thrombin was removed from the solution by adding in series a benzamidine column Amersham Biosciences). Protein purity and identity were confirmed by SDS−PAGE (Bio-Rad, Hercules, CA). The molecular mass for sytI C2AB is approximately 38 kDa, consisting of synaptotagmin residues 96−421 and 13 additional residues from the pGEX vector on the *N*-terminus. Following affinity purification, an additional purification step on an anion exchange column was performed as described previously (*18*). Pure fractions of C2AB, as indicated by an absorption maximum at 278 nm, were then buffer exchanged into 0.5 mM ammonium bicarbonate, vacuum desiccated, and stored at −20 °C. Protein concentration was determined by Bradford assay prior to its desiccation and was also measured gravimetrically. Protein purity and identity were confirmed by SDS−PAGE.

Spin Labeling sytI C2AB. The protein was spin-labeled as previously described using the sulfhydryl reactive spin label, (1-oxyl-2,2,5,5-tetramethyl-Δ^3-pyrroline-3-methyl) methanethiosulfonate (MTSL; Toronto Research Chemicals) (*18*) at a 1:3:30 mole ratio of protein/DTT/MTSL. Excess free spin label was removed by passing the sample through a HiPrep 26/10 desalting column (Amersham Biosciences). The spin-labeled protein was concentrated to 20−300 μM using Centripreps and Centricons (Millipore).

Large Unilamellar Vesicles. 1-Palmitoyl-2-oleoyl-*sn*-glycero-3-phosphocholine (POPC) and 1-palmitoyl-2-oleoyl-*sn*-glycero-3-phosphoserine (POPS) (Avanti Polar Lipids) were used to prepare large unilamellar vesicles (LUVs) with a POPC/POPS ratio of 3:1 as described previously (*17*).

Measurement of C2AB Metal Ion Affinities. Cation affinities of the spin-labeled C2AB mutants were measured with a terbium(III) fluorescence binding assay (*20*) as described previously (*18*). The change in tryptophan emission intensity due to energy transfer to Tb^{3+}, ΔF, was determined as a function of Tb^{3+} concentration and normalized to yield the fraction of metal ion sites bound, f_b, and a cation dissociation constant, K_d.

EPR Spectroscopy. EPR spectra were obtained and processed as before (*18*) from aqueous C2AB samples at protein concentrations ranging from 20 to 300 μM. Membrane-bound protein spectra were obtained under these same conditions but with the addition of LUVs (25 mM total lipid) to ensure complete membrane binding and low surface densities of the protein. Continuous-wave power saturation experiments were performed on each membrane-bound sytIC2AB mutant as described elsewhere (*21*) and used to calculate the depth parameter, Φ (*22*).

Modeling the Orientation and Position of the sytI C2A-(C2B) and C2B(C2A) Domains. Models for the orientation and position of the synaptotagmin I C2A and C2B were generated from the EPR depth parameters using an approach described in detail elsewhere (*17*, *21*). Briefly, the high-resolution solution structure of each domain, known depth calibration points, and an empirical form for the depth parameter Φ were fit to create the models of protein orientation and depth. As shown previously, Φ has a dependence upon depth that can be described by

$$\Phi = A \tanh[B(x - C)] + D \quad (1)$$

where x represents the distance of the label from the lipid phosphates. The values of A and D set the bulk values of Φ in water and hydrocarbon, C determines the position of the reflection point of the curve, and B determines the slope of the curve (*17*, *21*). To generate coordinates for modeling, the R1 side chain was appended to averaged high-resolution NMR structures of either C2A (pdb: 1BYN) or C2B (pdb: 1K5W) and placed in configurations, where the first, second, and third dihedral angles were in a g^+, g^+, $g^\pm$ conformation (*23*). Because of steric constraints, exceptions to this configuration were residues 202 (g^+, t, g^+) and 239 (g^+, t, g^-) for C2A(C2B) and 327 and 370 (g^+, t, g^+) for C2B(C2A). A set of coordinates for the nitrogen atom on the R1 side chain was generated and used for modeling.

RESULTS

C2AB Binds Strongly to the Metal Ion and Membranes. A Tb^{3+} fluorescence binding assay was used to determine the metal ion binding affinity as well as the membrane affinity of the C2AB fragment that was expressed and isolated here. Shown in Figure 2 are the metal binding curves obtained for C2AB in solution and in the presence of lipid vesicles composed of POPC and POPS, respectively. From the data in Figure 2a, the Tb^{3+} ion affinity to C2AB in solution is approximately 4 μM, and it increases to an affinity of 0.5 μM for the wild-type protein in the presence of POPC/POPS (75:25). The increase in affinity in the presence of membranes is due to membrane association of the C2AB fragment, and it may be used as a comparative measure of membrane affinity to test the function of the R1 mutants of C2AB (*18*, *20*) (Figure 2b). At subsaturating concentrations of Tb^{3+}, the titration of C2AB with POPC/POPS membranes yields a membrane-binding curve (Figure 2c) and a lipid affinity of 4.6 μM. This affinity is obtained in just 2 mol % POPS, and indicates strong binding to POPS containing bilayers.

Previously, a wide range of substitutions of the R1 side chain on the surface of C2A and C2B were tested for their metal- and membrane-binding affinity (*17*, *18*). In all cases, the C2A or C2B domains containing single R1 substitutions bound to metal ions and membranes, and these substitutions produced minimal perturbations on membrane affinity. A number of single R1 substitutions of C2AB were tested here for their ability to bind Tb^{3+} in the presence of membranes. A list of Tb^{3+} affinities for several C2AB R1 mutants as well as the values for the wild-type protein is shown in Table 1 . In each case, the R1 mutants that were produced bind with affinities comparable to those of the wild-type protein and indicate that these substitutions do not significantly alter C2AB membrane binding.

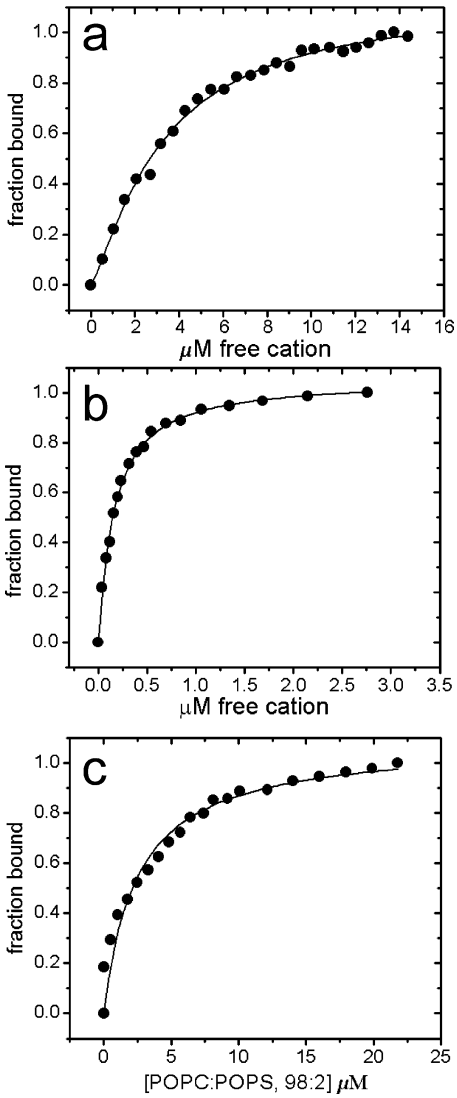

FIGURE 2: Tb^{3+} ion and membrane binding by the quenching of intrinsic tryptophan fluorescence. The plot of fraction bound vs free metal ion binding sites where the data are corrected for bound cations. (a) Binding of Tb^{3+} to wild-type C2AB in aqueous solution, where the fit (solid line) yields a $K_d = 4.3 \pm 0.3$ μM. (b) Binding of Tb^{3+} to the K327R1 mutant of C2AB in the presence of 50 uM of POPC/POPS (75:25) LUV, where the fit (solid line) yields a K_d of 0.16±0.006 μM. (c) The plot of fraction bound vs total lipid concentration. The lipid was added as POPC/POPS (98:2) LUV in 5 μM Tb^{3+}. When corrected for free lipid concentration, the fit to the data (solid line) yields a binding affinity of 4.6 ± 0.3 μM. A much lower concentration of POPS was used in this binding measurement because of the very high membrane affinity of sytIC2AB to membranes containing POPS. The protein concentration was 670 nM in (a) and 330 nM for (b) and (c). The data were fit by an independent site-binding isotherm with a Hill coefficient of $n = 1$.

First and Third Ca^{2+}-Binding Loops of Each Domain Penetrate POPC/POPS Bilayers. Figure 3 shows the X-band EPR spectra for R1 mutants of C2AB in the presence of Ca^{2+} in solution and in the presence of POPC/POPS bilayers. Most of these spectra arise from nitroxides that are executing relatively fast (ns) isotropic motion, characteristic of nitroxides that are not sterically constrained and attached to flexible backbone segments. This is expected because most of these labels are placed within or near the three Ca^{2+}-binding loops of C2A or C2B (Figure 1). When added to POPC/POPS bilayers, the EPR spectra for labels at a number of positions

Table 1: Tb^{3+} Binding to C2AB in the Presence of POPC/POPS Vesicles[a]

C2AB	K_d
wild-type	$0.52 \pm 0.04\ \mu M$
K297R1	$0.28 \pm 0.15\ \mu M$
T334R1	$0.24 \pm 0.18\ \mu M$
N370R1	$0.10 \pm 0.01\ \mu M$
G368R1	$0.07 \pm 0.01\ \mu M$
K369R1	$0.72 \pm 0.02\ \mu M$
I367R1	$0.2 \pm 0.05\ \mu M$
K327R1	$0.16 \pm 0.006\ \mu M$

[a] The Tb^{3+} affinities were obtained in the presence of 50 μM POPC/POPS (75:25). The values of *n*, the Hill coefficient, were allowed to vary in the fit and ranged between 0.7 and 2.3.

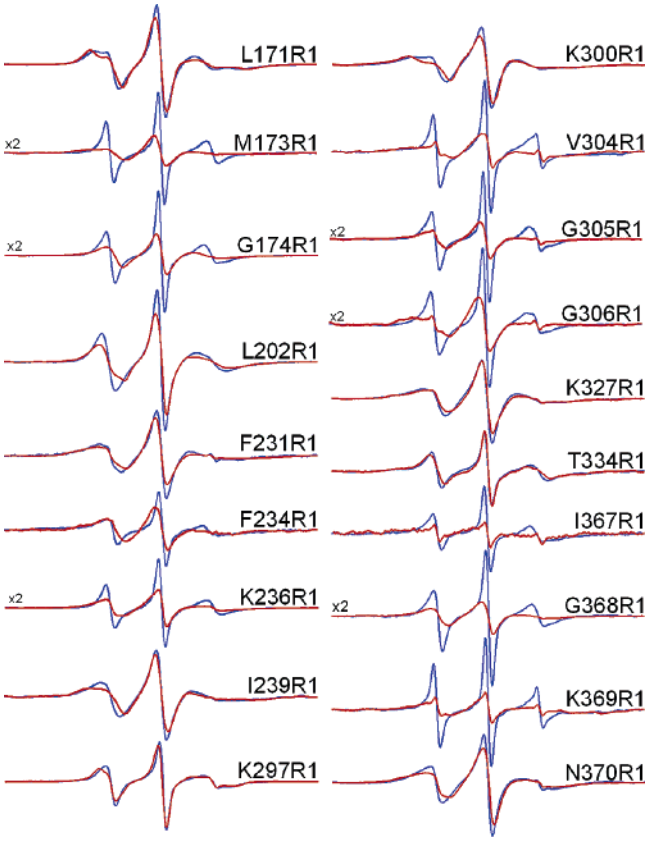

FIGURE 3: X-band EPR spectra of single R1 substitutions in sytIC2AB in the presence of Ca^{2+}. Aqueous spectra are shown in blue, and the spectra of C2AB completely bound to POPC/POPS (75:25) vesicles are shown in red. Spectra are normalized against the total spin number so that the amplitudes provide an approximate measure of the motional averaging of the R1 side chain. Loop sites that insert into the bilayer show the most dramatic changes in line shape upon membrane binding. The spectra are all 100 Gauss scans.

show significant broadening and a decrease in their normalized amplitudes. The most dramatic changes are associated with labels at positions within the first (M173R1, G174R1) and third (K236R1) Ca^{2+}-binding loops of C2A and the first (V304R1, G305R1, and G306R1) and third (I367R1, G368R1, and K369R1) Ca^{2+}-binding loops of C2B. This broadening results from a decrease in both the rates and amplitudes of motion of the R1 side chain. Previously, changes in the EPR spectra of spin-labeled C2 domains were shown to be associated with the penetration of these labeled sites into the membrane interface (*17*, *18*, *21*). The source of this broadening is not entirely clear, but it could result from changes in backbone dynamics, loop structure, or interactions

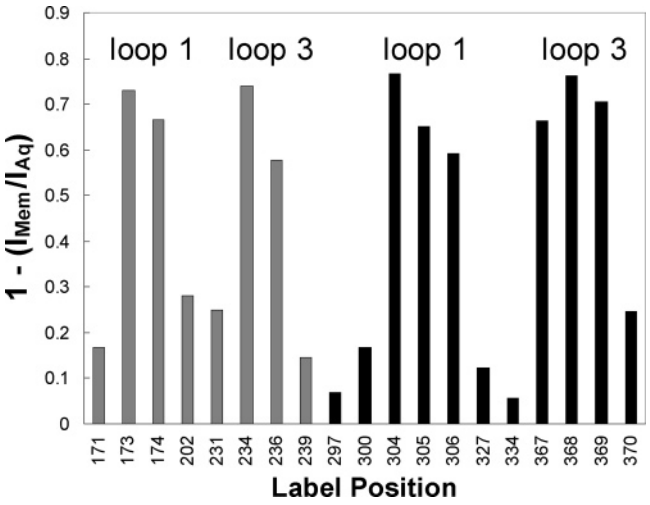

FIGURE 4: Change in normalized EPR amplitudes upon membrane binding. Normalized amplitudes are plotted as $1 - (I_{mem}/I_{aq})$, where I_{mem} is the amplitude bound to membranes, and I_{aq} is the amplitude in solution. Mutants in C2A, gray; mutants in C2B, black. Larger values indicate the greatest loss of motional averaging upon membrane binding.

made between the membrane-binding loops and lipids in the interface. The changes in the EPR spectra that are seen in Figure 3 upon membrane addition are not seen in the absence of Ca^{2+} and indicate that there is Ca^{2+}-dependent membrane penetration of sites in both C2A and C2B to membranes containing POPS.

The normalized amplitudes of the EPR spectra provide a qualitative comparison of the rates of motion of the nitroxide side-chain, and Figure 4 plots the change in the normalized amplitude for each of the 19 R1 mutants in the presence and absence of bilayers. Four regions yield spectra that show the most significant change in line shape upon membrane binding, and these include the first and third Ca^{2+}-binding loops of each domain.

EPR spectra for each of the 19 spin-labeled sytIC2AB mutants were power saturated in the presence of oxygen or Ni(II)EDDA to obtain a depth parameter, Φ, which is related to the position of the nitroxide relative to the membrane interface. Table 2 lists these parameters, along with depth parameters obtained for C2A or C2B alone as isolated domains. Values of Φ of -2.0 to -2.5 are associated with labels having aqueous exposure and lying more than 5 Å on the aqueous side of the membrane interface. Values greater than this are localized in the interface or within the bilayer interior. The most positive values are associated with labels in Ca^{2+}-binding loops one and three of C2A and C2B.

SytIC2AB Penetrates More Deeply than Either C2A or C2B Alone. Figure 5 compares EPR spectra obtained for several sites in sytIC2AB (blue traces) with spectra obtained previously (*17*, *18*) for the same positions in either C2A or C2B (red traces). At most sites, the spectra are virtually identical in either the presence or absence of membranes. Spectra from spin labels placed in C2A are very similar when the isolated and tandem domains are compared, except for the spectrum from site M173R1, which is broader in the tandem domain than the isolated domain. This may result from differences in tertiary structure or backbone dynamics between the two expressed proteins, or a deeper penetration of C2A in the tandem construct. Sites in C2B exhibit more

Table 2: Depth Parameters, Φ, for C2AB or Isolated Domains[a]

mutant	C2AB	C2A,C2B	mutant	C2AB	C2B
L171R1	−1.9 ± 0.5	−1.7	V304R1	−0.4 ± 0.2	−1.5
M173R1	+0.8 ± 0.3	−1.4	G305R1	+0.8 ± 0.2	−0.7
G174R1	+0.6 ± 0.1	+0.4	G306R1	+0.3 ± 0.3	
L202R1	−2.5 ± 0.1	−2.4	K327R1	−2.2 ± 0.2	
F231R1	−1.4 ± 0.5	−1.7	T334R1	−2.2 ± 0.1	−2.2
F234R1	−0.1 ± 0.1	+0.6	I367R1	−2.1 ± 0.4	
K236R1	−0.3 ± 0.2	−0.6	G368R1	+0.6 ± 0.1	−1.8
I239R1	−1.5 ± 0.3	−2.1	K369R1	−1.2 ± 0.2	−2.3
K297R1	−2.4 ± 0.1		N370R1	−2.3 ± 0.3	−2.2
K300R1	−1.7 ± 0.3				

[a] The depth parameters for C2AB are the average of two to four measurements, and errors represent standard deviations for the data. Data listed for C2A and C2B were reported in refs 17 and 18 (*17, 18*), respectively and are shown for comparison. Errors in Φ for the isolated domains are ±0.2 to 0.4. Π^{oxy} and Π^{NiEDDA} have an uncertainty of ±0.05 and ±0.4, respectively. For comparison, the depth parameter for the spin-labeled lipid 5-doxyl PC is +1.49 ± 0.15. A listing of depth parameters for other lipid and bacteriorhodopsin spin labels used in the fitting of eq. 1 was published previously (*21*).

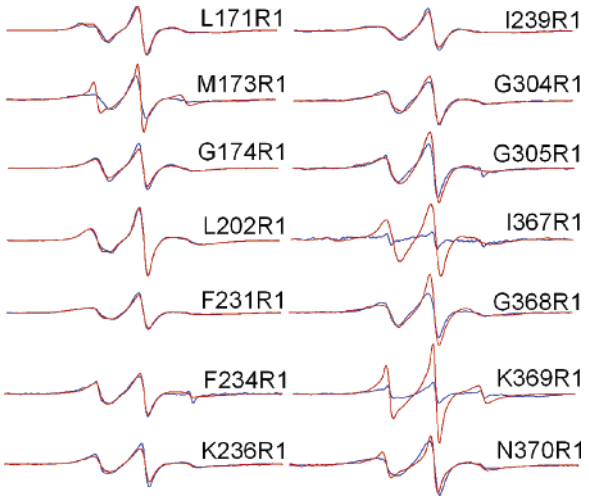

FIGURE 5: Comparison of EPR spectra from tandem and isolated C2domains. X-band EPR spectra of R1-labeled sytIC2AB (blue traces) or separately expressed sytIC2A or sytIC2B (red traces) when the domains are fully bound to POPC/POPS (3:1) membranes in the presence of Ca^{2+}.

differences when the isolated and tandem domains are compared, and a few of these differences are quite dramatic. For example, I367R1 and K369R1 are significantly broadened when C2A and C2B are present together. This difference is not the result of dipole−dipole interactions between spin labels because dilution with unlabeled wild-type C2AB does not alter these spectra. These differences must be due to differences in membrane penetration, structural rearrangements in the third Ca^{2+}-binding loop, or altered interactions with membrane lipid.

The depth parameters shown in Table 2 indicate that many sites in C2A and C2B penetrate more deeply when present together (in sytIC2AB) than as isolated domains. At most sites with full aqueous exposure (for example, L202R1, T334R1, and N370R1), the depth parameters are unchanged when each isolated domain is compared to sytIC2AB. However, most labels that are located in loop regions show significantly greater depth parameters, indicating greater membrane penetration in sytIC2AB than in either isolated domain (for example, M173R1, V304R1, G305R1, and G368R1). Taken together, both the spectra and depth

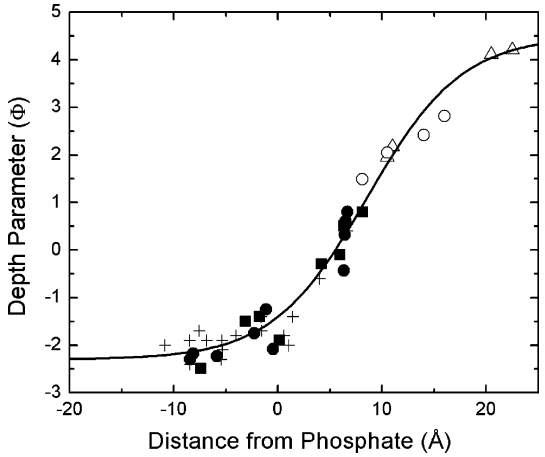

FIGURE 6: Fit obtained with depth parameters by orienting sytI C2A and C2B. The orientation and position of C2A and C2B in sytIC2AB are oriented until a best fit is obtained between measured depth parameters (sytIC2AB (C2A)(■), sytIC2AB (C2B) (●)), calibration data (open figures bacteriorhodospin (Δ), doxyl-labeled phosphatidylcholine (○) sytIC2A (+)), and a calibration curve. The solid line represents the calibration curve, which is described by eq 1, where *A, B, C,* and *D* are 3.4, 0.11, 8.56, and 1.1, respectively.

parameters indicate that C2A and C2B interact differently with the membrane interface when present in tandem than they do as isolated domains. In particular, the data suggest that C2A and C2B penetrate more deeply in sytIC2AB.

Membrane Orientation and Depth of Penetration of sytIC2AB. The depth parameters shown in Table 2 were used to determine the membrane orientations and positions of C2A and C2B for sytIC2AB. The procedure (see Material Methods) was identical to that applied previously for the isolated C2A and C2B and treated each domain as a static rigid structure. The best fit obtained for the depth data from C2A and C2B, the orientations of the domains, and the depth dependence of Φ are shown in Figure 6 .

The fit shown in Figure 6 yields the depth and position for C2A and C2B shown in Figure 7a. Also shown for comparison are the membrane positions determined previously for the isolated C2A and C2B domains (Figure 7b). As indicated by the primary data, the membrane interactions made by both domains take place primarily through the first and third Ca^{2+}-binding loops. The orientations are similar to those seen for the isolated domains, but both domains are tilted in sytIC2AB so that the axis of the domains defined by the β-sheets is aligned closer to the bilayer normal. The orientation seen for C2B places its polybasic strand off the bilayer interface. Compared to the isolated domains, both domains in C2AB appear to lie approximately 6−7 Å deeper in the bilayer interface. The largest uncertainly in the depth arises from the uncertainly in R1 side chain configuration, and a careful analysis of the effect of side chain orientation indicates that the error in determining the depth of penetration is on the order of ±2 Å. Although not large compared to the error, the differences between the depth of penetration of C2AB compared to C2A or C2B appear to be significant. This is also indicated by the fact that both domains are translocated inward by about the same extent in C2AB and by the fact that the primary data (EPR spectra and depth parameters) indicate deeper penetration of sytIC2AB.

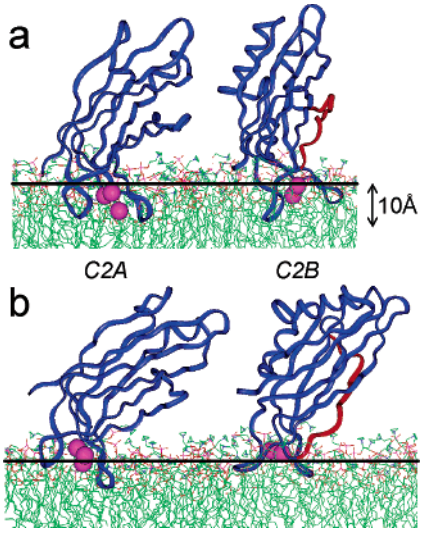

FIGURE 7: Position and docking of synaptotagmin C2 domains at the membrane interface. (a) Positions obtained for C2A and C2B in sytIC2AB at the membrane interface obtained from the fit in Figure 6**.** The membrane docked structures were produced using pdb structure files for C2A and C2B: pdb ID: 1BYN and pdb ID: 1K5W, respectively. The best fit positions correspond to successive Euler angle rotations for the ϕ (z-axis), θ (x'-axis), and ψ (z'-axis) of 41°, 143°, and 298°, respectively, a displacement of structure along the x-axis of −10.1 Å for C2A and 58°, 132°, and 284°, respectively, and a displacement of structure along the x-axis of −16.3 Å for C2B. These rotations and displacements are carried out using the center-of-mass of the protein on the local coordinate frame defined by the pdb file, where the bilayer phosphates lie in the $y-z$ plane (solid line). (b) Orientation and position of sytIC2A and sytIC2B determined previously (*17*, *18*). The highly positively charged (polybasic) region of C2B is shown in red.

DISCUSSION

At the present time, the precise role of synaptotagmin I in the fusion process is not known. Synaptotagmin I may promote fusion by directly interacting with SNAREs or by targeting the plasma (or vesicle) membrane in a Ca^{2+}-dependent fashion. However, C2 domains are known to function as Ca^{2+}-dependent membrane-binding modules, and Ca^{2+}-dependent membrane insertion could provide the trigger for fusion. Our goals in this work were to determine the membrane docking position of sytIC2AB in membranes containing POPC/POPS and to determine whether the interactions differed from those made by each isolated domain.

The data presented here indicate that C2A and C2B make similar contacts with the membrane interface either as isolated domains or in a tandem construct. Like the isolated domains (*17*, *18*), both C2A and C2B contact POPC/POPS membranes through interactions made by their first and third Ca^{2+}-binding loops. Several features regarding the position of sytIC2AB deserve note. First, the orientation of C2B places its highly positively charged basic strand away from the membrane interface. This indicates that this strand does not closely interact with the POPS in the bilayer interface and that electrostatic interactions by this strand do not dominate the interaction of C2B with the interface when it is attached to POPC/POPS in a Ca^{2+}-dependent manner. It is interesting to consider the possibility that this strand may be available for interactions with other components in the fusion system and that this orientation might allow for simultaneous membrane/SNARE interactions. C2B is also reported to bind strongly to membranes containing PI(4,5)P_2 (*13*). Conceivably, this interaction with PI(4,5)P_2 might act to modulate the orientation and availability of the polybasic face of C2B for other interactions.

A recent report provides evidence that this region of C2B inserts into bilayers, providing a mechanism for C2B to bridge between two bilayers in a Ca^{2+}-dependent fashion (*24*). However, we do not see evidence for this penetration in these data, and the EPR data are quite clear in this regard. One spin label we have in this region, K327R1, does not exhibit line shape changes upon membrane association that would accompany insertion, and the collision depth parameters indicate an aqueous exposure for this site when membrane bound. We are currently exploring this region in greater detail. It is conceivable that the polybasic region makes a peripheral interaction with a membrane interface, as has been observed for many basic peptides (*25*−*28*). If this association were localized to the double-layer and our spin label was 5 Å or greater off the bilayer surface, our current choice of collision reagents might not detect the interaction.

The data presented above indicate that there are differences in the extent of membrane penetration made by the two domains when present in the tandem construct. Although there is considerable uncertainty in our analysis, the differences in depth appear to be significant as judged by the models generated and by the primary data. Previous work using fluorescence demonstrated in a very qualitative way that C2B as an isolated domain failed to penetrate bilayers, but it penetrated when present in tandem with C2A (*6*, *29*). The results presented here and elsewhere (*18*) indicate that although there is penetration of C2B in the absence of C2A, there is deeper membrane penetration in the tandem domain than the isolated domains. Therefore, our findings regarding C2B are qualitatively consistent with the earlier work.

It is not clear why tandem domains would act synergistically to enhance their mutual penetration, but a number of possibilities exist. These domains may alter lipid curvature strain and could promote their own membrane association, as has been observed for some surface-interacting peptides (*30*, *31*). An interesting possibility is that the C2 domains of sytI might promote a lateral phase separation and demixing of lipids such as phosphatidylserine (PS) and do so more efficiently when both domains are present. Indeed, previous work has provided evidence that C2A may demix lipids such as PS in bilayers (*20*). Increasing the local concentration of PS would increase the long-range electrostatic interaction between C2AB and the membrane interface and might facilitate a deeper membrane penetration.

As indicated above, membrane fusion may be facilitated or triggered by the membrane insertion of C2 domains. Insertion of the domains could destabilize the bilayer by promoting lipid demixing of PS and other charged lipids such as PI(4,5)P_2. In addition to lipid demixing, membrane penetration of the C2 domains of sytI alone may be disruptive of bilayer packing. Indeed, fusion peptides have been shown to reside in the membrane interface (*32*) in a fashion that is thought to thin bilayers and be highly disruptive of membrane packing (*33*−*35*).

In summary, the membrane interactions and position of the two C2 domains, a soluble fragment of synaptotagmin I, have been determined by site-directed spin labeling. The

data indicate that these domains interact with bilayers primarily through their first and third Ca^{2+}-binding loops and that the highly polybasic face of C2B does not closely interact with the interface of PS-containing membranes. Compared to each C2 domain when studied alone, the domains when present in tandem appear to penetrate more deeply into the interface, indicating that there are cooperative interactions modulating membrane insertion. These cooperative interactions between C2 domains may provide an explanation for the appearance of multiple C2 domains in synaptotagmin and other proteins that are involved in membrane trafficking and repair.

ACKNOWLEDGMENT

We thank Dr. April Frazier for help with the initial production and purification of sytIC2AB.

REFERENCES

1. Jahn, R., Lang, T., and Sudhof, T. C. (2003) Membrane fusion, *Cell 112*, 519−533.
2. Rothman, J. E. (1994) Mechanisms of intracellular protein transport, *Nature 372*, 55−63.
3. Sollner, T. H. (2003) Regulated exocytosis and SNARE function, *Mol. Membr. Biol. 20*, 209−220.
4. Koh, T. W., and Bellen, H. J. (2003) Synaptotagmin I, a Ca2+ sensor for neurotransmitter release, *Trends. Neurosci. 26*, 413−22.
5. Chapman, E. R., An, S., Edwardson, J. M., and Jahn, R. (1996) A novel function for the second C2 domain of synaptotagmin. Ca^{2+}-triggered dimerization, *J. Biol. Chem. 271*, 5844−5849.
6. Bai, J., and Chapman, E. R. (2004) The C2 domains of synaptotagmin−partners in exocytosis, *Trends Biochem. Sci. 29*, 143−51.
7. Sutton, R. B., Ernst, J. A., and Brunger, A. T. (1999) Crystal structure of the cytosolic C2A-C2B domains of synaptotagmin III: implications for Ca^{2+}-independent SNARE complex interaction, *J. Cell Biol. 147*, 589−598.
8. Tomsig, J. L., and Creutz, C. E. (2000) Biochemical characterization of copine: a ubiquitous Ca2+-dependent phospholipid-binding protein, *Biochemistry 39*, 16163−16175.
9. Schulz, T. A., and Creutz, C. E. (2004) The tricalbin C2 domains: lipid-binding properties of a novel, synaptotagmin-like yeast protein family, *Biochemistry 43*, 3987−95.
10. Bansal, D., and Campbell, K. P. (2004) Dysferlin and the plasma membrane repair in muscular dystrophy, *Trends Cell Biol. 14*, 206−13.
11. Davis, D. B., Doherty, K. R., Delmonte, A. J., and McNally, E. M. (2002) Calcium-sensitive phospholipid binding properties of normal and mutant ferlin C2 domains, *J. Biol. Chem. 277*, 22883−8.
12. Doherty, K. R., and McNally, E. M. (2003) Repairing the tears: dysferlin in muscle membrane repair, *Trends Mol. Med. 9*, 327−30.
13. Bai, J., Tucker, W. C., and Chapman, E. R. (2004) PIP_2 increases the speed of response of synaptotagmin and steers its membrane-penetration activity toward the plasma membrane, *Nat. Struct. Mol. Biol. 11*, 36−44.
14. Damer, C. K., and Creutz, C. E. (1994) Synergistic membrane interactions of the two C2 domains of synaptotagmin, *J. Biol. Chem. 49*, 31115−31123.
15. Tucker, W. C., Weber, T., and Chapman, E. R. (2004) Reconstitution of Ca^{2+}-regulated membrane fusion by synaptotagmin and SNAREs, *Science 304*, 435−438.
16. Wang, C. T., Lu, J. C., Bai, J., Chang, P. Y., Martin, T. F., Chapman, E. R., and Jackson, M. B. (2003) Different domains of synaptotagmin control the choice between kiss-and-run and full fusion, *Nature 424*, 943−7.
17. Frazier, A. A., Roller, C. R., Havelka, J. J., Hinderliter, A., and Cafiso, D. S. (2003) Membrane-bound orientation and position of the synaptotagmin I C2A domain by site-directed spin labeling, *Biochemistry 42*, 96−105.
18. Rufener, E., Frazier, A. A., Wieser, C. M., Hinderliter, A., and Cafiso, D. S. (2005) Membrane-bound orientation and position of the synaptotagmin C2B domain determined by site-directed spin labeling, *Biochemistry 44*, 18−28.
19. Sambrook, J., Fritsch, E. F., and Maniatis, T. (1989) *Molecular Cloning: A Laboratory Manual*, Cold Spring Harbor Press, Plainview, NY.
20. Hinderliter, A., Almeida, P. F. F., Creutz, C. E., and Biltonen, R. L. (2001) Domain formation in a fluid mixed lipid bilayer modulated through binding of the C2 protein motif, *Biochemistry 40*, 4181−4191.
21. Frazier, A. A., Wisner, M. A., Malmberg, N. J., Victor, K. G., Fanucci, G. E., Nalefski, E. A., Falke, J. J., and Cafiso, D. S. (2002) Membrane orientation and position of the C2 domain from cPLA2 by site-directed spin labeling, *Biochemistry 41*, 6282−6292.
22. Altenbach, C., Greenhalgh, D. A., Khorana, H. G., and Hubbell, W. L. (1994) A collision gradient-method to determine the immersion depth of nitroxides in lipid bilayers. Application to spin-labeled mutants of bacteriorhodopsin, *Proc. Natl. Acad. Sci. U S A 91*, 1667−1671.
23. Langen, R., Oh, K. J., Cascio, D., and Hubbell, W. L. (2000) Crystal structures of spin-labeled T4 lysozyme mutants: implications for the interpretation of EPR spectra in terms of structure, *Biochemistry 39*, 8396−8405.
24. Arac, D., Chen, X., Khant, H. A., Ubach, J., Ludtke, S. J., Kikkawa, M., Johnson, A. E., Chiu, W., Sudhof, T. C., and Rizo, J. (2006) Close membrane-membrane proximity induced by Ca(2+)-dependent multivalent binding of synaptotagmin-1 to phospholipids, *Nat. Struct. Mol. Biol. 13*, 209−217.
25. Ben-Tal, N., Honig, B., Miller, C., and McLaughlin, S. (1997) Electrostatic binding of proteins to membranes. Theoretical predictions and experimental results with charybdotoxin and phospholipid vesicles, *Biophys. J. 73*, 1717−1727.
26. Murray, D., Arbuzova, A., Hangyas-Mihalyne, G., Gambhir, A., Ben-Tal, N., Honig, B., and McLaughlin, S. (1999) Electrostatic properties of membranes containing acidic lipids and adsorbed basic peptides: theory and experiment, *Biophys. J. 77*, 3176−3188.
27. Victor, K., Jacob, J., and Cafiso, D. S. (1999) Interactions controlling the membrane binding of basic protein domains, *Biochemistry 38*, 12527−12536.
28. Victor, K. G., and Cafiso, D. S. (2001) Location and dynamics of basic peptides at the membrane interface: electron paramagnetic resonance spectroscopy of tetramethyl-piperidine-N-oxyl-4-amino-4-carboxylic acid-labeled peptides, *Biophys. J. 81*, 2241−2250.
29. Bai, J., Wang, P., and Chapman, E. R. (2002) C2A activates a cryptic Ca(2+)-triggered membrane penetration activity within the C2B domain of synaptotagmin I, *Proc. Natl. Acad. Sci. U.S.A. 99*, 1665−1670.
30. Archer, S. J., Ellena, J. F., and Cafiso, D. S. (1991) Dynamics and aggregation of the peptide ion channel alamethicin. Measurements using spin-labeled peptides, *Biophys. J. 60*, 389−398.
31. Lewis, J. R., and Cafiso, D. S. (1999) Correlation between the free energy of a channel-forming voltage-gated peptide and the spontaneous curvature of bilayer lipids, *Biochemistry 38*, 5932−5838.
32. Han, X., Bushweller, J. H., Cafiso, D. S., and Tamm, L. K. (2001) Membrane structure and fusion-triggering conformational change of the fusion domain from influenza hemagglutinin, *Nat. Struct. Biol. 8*, 715−20.
33. Lague, P., Roux, B., and Pastor, R. W. (2005) Molecular dynamics simulations of the influenza hemagglutinin fusion peptide in micelles and bilayers: conformational analysis of peptide and lipids, *J. Mol. Biol. 354*, 1129−1141.
34. Vaccaro, L., Cross, K. J., Kleinjung, J., Straus, S. K., Thomas, D. J., Wharton, S. A., Skehel, J. J., and Fraternali, F. (2005) Plasticity of influenza haemagglutinin fusion peptides and their interaction with lipid bilayers, *Biophys. J. 88*, 25−36.
35. Zemel, A., Ben-Shaul, A., and May, S. (2004) Membrane perturbation induced by interfacially adsorbed peptides, *Biophys. J. 86*, 3607−3619.

BI060874J